J Pharmacol Sci **124**, 18 – 30 (2014)

Journal of Pharmacological Sciences

Full Paper

Tranilast Alleviates Endothelial Dysfunctions and Insulin Resistance via Preserving Glutathione Peroxidase 1 in Rats Fed a High-Fat Emulsion

Xuan Yang[1,*], Lei Feng[2], Changjiang Li[3], and Yu Li[4]

[1]*Department of Cardiology,* [2]*Diagnostic Imaging Division, Qingdao Municipal Hospital, Qingdao 266000, Shandong, China*
[3]*Intensive Care Unit, Qingdao Central Hospital, Qingdao 266042, Shandong, China*
[4]*Department of Internal Medicine, Zibo Municipal Hospital Authorities, Zibo 255000, Shandong, China*

Received August 26, 2103; Accepted September 30, 2013

Abstract. We investigated the effects of treatment with tranilast on vascular and metabolic dysfunction induced by a high-fat emulsion intragastric administration. Wistar rats were randomized to receive water or high-fat emulsion with or without tranilast treatment (400 mg/kg per day) for 4 weeks. Insulin sensitivity was determined with a hyperinsulinemic-euglycemic clamp experiment and short insulin tolerance test. Vascular reactivity was evaluated using aortic rings in organ chambers. Glutathione peroxidase 1 (GPX1) expressions, eNOS phosphorylation and activity, MCP-1, H_2O_2 formation, and NO production were determined in vascular or soleus tissues. Tranilast treatment was found to prevent alterations in vascular reactivity and insulin sensitivity and to prevent increases in plasma glucose and insulin noted in the high-fat emulsion–treated rats. These were associated with increased antioxidant enzyme GPX1 expression, eNOS phosphorylation and activity, and NO production, but reductions in H_2O_2 accumulation. Moreover, tranilast preserved GPX1 expression in palmitic acid (PA)-treated endothelial cells with a consequent decreased ROS formation and increased eNOS phosphorylation and NO production. Therefore, oxidative stress induced by a relatively short-term high-fat diet could cause the early development of vascular and metabolic abnormalities in rats, and tranilast has a beneficial effect in vascular dysfunctions and insulin resistance via preserving GPX1 and alleviating oxidative stress.

Keywords: insulin resistance, oxidative stress, endothelial dysfunction, tranilast, metabolic syndrome

Introduction

Atherosclerosis (also known as arteriosclerotic vascular disease) is a chronic inflammatory response to high fatty materials such as free fatty acids, cholesterol, and triglyceride, leading to plaque formation and hardening of the arteries. Dyslipidemia associated with the metabolic syndrome is one of the most important risk factors associated with atherosclerosis apart from smoking, hypertension, diabetes mellitus, and other causes (1). The possibility of retarding human atherosclerosis or even inducing its regression is one of the present therapeutic challenges. Endothelium is an impermeable inner covering of the blood vessels and its integrity is important in restraining leukocyte adhesion, inhibiting inflammation, and supporting the vasculature during hemodynamic stresses and oxidative stress (2). The endothelial function status represents an comprehensive index of both the primary cardiovascular risk factor burden and the sum of all vascular protection factors in any given individual (3). Endothelial dysfunction, characterized by reduced NO bioavailability and increased oxidative stress, is regarded as an early critical event in atherogenesis (4) and precedes development of clinically detectable plaques in the coronary arteries (5). It is also considered an important event in the development of micro vascular complications in metabolic syndrome (6). Currently, lowering serum lipids using statins is the primary treatment to preserve the endothelium. However, the development of new pharmacological drugs that affect multiple targets such as oxidative stress and inflammation may provide better protection against atherosclerosis.

*Corresponding author. yangxuan4040@163.com
Published online in J-STAGE on December 27, 2013
doi: 10.1254/jphs.13151FP

Tranilast, *N*-(3,4-dimethoxycinnamoyl) anthranillic acid, is used as an anti-allergic agent primarily to treat allergic diseases such as bronchial asthma, atopic dermatitis, and allergic rhinitis (7, 8). Tranilast exerts anti-inflammatory and anti-angiogenesis effects via inhibiting expression of TGF-β, MCP-1, and antigen-induced IL-2 lymphocyte responsiveness. It also has a certain anti-oxidant activity (7). Intriguingly, recent studies suggested that tranilast has cardiovascular-protective effects. Matsumura et al. (8) suggested that tranilast suppresses atherosclerotic development in Watanabe heritable hyperlipidemic rabbits. Saiura et al. (9) demonstrated that tranilast suppresses transplant-associated coronary arteriosclerosis in a murine model of cardiac transplantation. Moreover, tranilast was considered as a novel weapon against insulin resistance (7). Despite its increasing clinical use and potential importance, little is known of the underlying mechanism of its anti-anthrogenic properties.

Oxidative stress is a potent pathogenic mechanism in atherosclerosis (10) by promoting cellular injury, mitochondria dysfunction, and apoptosis (11). Antioxidant glutathione peroxidase 1 (GPX1) represents the pivotal antioxidant enzyme in vascular endothelium and exerts a protective effect against the presence of coronary artery disease (12). GPX1-deficient mice have endothelial dysfunction and abnormal cardiac function after ischemia/reperfusion injury (13, 14). So far, few studies have been conducted to elucidate the regulatory role that tranilast may play on protecting tissue antioxidant defensives and endothelial function.

Therefore, in the current studies we have examined the protective effects of tranilast in endothelial cells against high-fat diet / high FFA–induced cellular oxidative stress. Our major focus is to determine whether tranilast i) promotes the expression of antioxidant enzymes that can detoxify toxic free radicals, ii) executes it protective effects through the eNOS/NO pathway, and iii) preserves endothelial functions. The results of the present study provide further evidences for a functional role of tranilast in endothelial cells in relation to the prevention of atherosclerosis.

Materials and Methods

Materials

Rabbit polyclonal phospho-eNOS (Ser1177) was purchased from Cell Signaling. Rabbit polyclonal eNOS antibody was obtained from Abcam. Anti-MCP-1 and mouse monoclonal actin antibodies were obtained from Chemicon International, Inc. (Temecula, CA, USA). Tranilast, palmitic acid (PA), PEG-catalase, and BSA were purchased from Sigma (St. Louis, MO, USA). Horseradish peroxidase–conjugated anti-rabbit and anti-mouse secondary antibodies were purchased from Santa Cruz Biotechnology (Santa Cruz, CA, USA). Insulin was purchased from the First Biochemical Drug Company (Shanghai, China).

Preparation of fat emulsion

High-fat emulsion (HFE) diet was prepared as previously described (15). A constant volume of 100 mL fat emulsion containing 20 g lard, 1 g thyreostat, 5 g cholesterol, 1 g sodium glutamate, 5 g sucrose, and 5 g saccharose; 20 mL Tween 80; and 30 mL propylene glycol was prepared by adding distilled water and stored at 4°C.

Animals

Male Wistar rats weighing 180 – 220 g, 6-week-old, were obtained from Department of Animals, Shandong University. Animal studies were conducted using protocols approved by the Animal Care and Handling Committee of Shandong University. The rats were individually housed in a light-controlled [12-h (light) / 12-h (dark) cycle starting at 0600 h] and temperature-regulated (20°C – 22°C) space. The animals were allowed to acclimate to their environmental conditions and diets for 4 weeks before the experiments were initiated. Sixty Wistar rats were randomly divided into the normal control group and HFE group, 30/group. Rats in the normal control group received common water; rats in the HFE group were orally treated with the HFE (10 ml/kg) once per day for 4 weeks. At the beginning of diet intervention, one subgroup of water-treated rats (n = 15) and one subgroup of HFE-fed rats (n = 15) received tranilast by oral gavage at a dose of 400 mg/kg per day for the duration of the diet. The other subgroups of HFE-fed (n = 15) and water-treated (n = 15) rats did not receive tranilast, but were treated with the vehicle (0.2 mM phosphate buffer saline) by oral gavage. Body mass and food intake were recorded every 2 days.

Tissue collection for in vitro studies

The overnight-fasted rats were anesthetized with sodium pentobarbital (75 mg/kg, i.p.) and had their soleus muscles rapidly dissected out, weighed, and immediately processed for GPX1 protein assays and oxidant level measurements. The thoracic aortas (from the diaphragm to the aortic arch) were removed and cleaned of blood and surrounding adipose tissues. The vessels were either snap frozen and stored at −80°C or immediately processed for in vitro vascular reactivity studies. Visceral fat mass was assessed by weighing the total perirenal and peri-epididymal adipose tissues after dissection.

Glucose, insulin, triglycerides, and nonesterified fatty acids (NEFA) measurements

Plasma glucose concentrations were measured by the glucose oxidase method (16), using a Beckman glucose analyzer (Beckman Instruments, Palo Alto, CA, USA). Insulin levels were determined by radioimmunoassay (RIA) with porcine insulin standards and polyethylene glycol for separation (17). Plasma triglycerides were assayed by an enzymatic method (18), with a commercial kit from Roche Diagnostics, Ltd. (Shanghai, China) that allowed correction for free glycerol. Plasma NEFA were measured with commercially available kits (Wako Chemicals, Dallas, TX, USA).

Measurement of endothelium-dependent and endothelium-independent vasorelaxation

The effects of HFE diet and tranilast treatment on vascular reactivity were evaluated in vitro using aortic rings in organ chambers (PowerLab; AD Instruments, Colorado Springs, CO, USA) as described previously (19, 20). The aortic rings were allowed to equilibrate for 1 h in a Krebs-Henseleit physiological solution containing 25 mM $NaHCO_3$, 1.18 mM KH_2PO_4, 2.5 mM $CaCl_2$, 1.18 mM $MgSO_4$, 118 mM NaCl, 4.7 mM KCl, and 5.5 mM glucose. The arteries were then constricted in a high-potassium Krebs solution containing 18 mM KCl and re-equilibrated. The baths were then rinsed 3 times with Krebs solution followed by equilibration. Subsequently, the aortic rings were constricted with 10^{-6} M phenylephrine (Sigma). To ensure the endothelium was functioning, the endothelium-dependent dilator responses to 10^{-5} M carbachol (Sigma) were obtained while the rings were constricted. After washout of the carbachol and phenylephrine, a cumulative dose–response curve to phenylephrine (10^{-9} – 10^{-5} M) was obtained. To assess endothelium-dependent and endothelium-independent vasorelaxation, the aortic rings were constricted with phenylephrine (10^{-6} M), and cumulative relaxation curves to carbachol (10^{-8} – 10^{-4} M) and then to sodium nitroprusside (SNP) (10^{-10} – 10^{-7} L, Sigma) were quantified.

Cell culture and transfection

Rat aortic endothelial cells (RAOEC; Cell Applications, San Diego, CA, USA) were cultured in RAOEC growth medium (Cell Applications) at 37°C in a 5% CO_2 humidified incubator. RAOEC at passage 6 were used. The transfected cells were used 48 h after transfection with pcDNA3.1/GPX1 using TransPass Endothelial Cell Transfection Reagent (New England Biolabs), and 70% – 80% transfection efficiency was typically achieved.

For constructing pcDNA3.1/GPX1, we synthesized the polynucleotides 5′-CATCCCAAGCTTACAGTG CTTGTTCGGGGCGCTCGGCTGGCTTCTTGGA CAATTGCGCCATGTGTGCTGCTCGGCTAGCTAG TAGTAGC-3′ and its complementary strand. This synthesized DNA fragment contained two restriction enzyme sites, HindIII and NheI. The nucleotides between the two sites are the same sequence, corresponding to 48 nucleotides of the 5′-noncoding region and 20 nucleotides of the coding region from the ATG start codon of the published human GPX1 cDNA sequence (21). In addition, there is a NheI site at nucleotide 20 from the ATG start codon in the GPX1 cDNA. The two 89-mer polynucleotide strands were annealed, and then this DNA fragment was cut using HindIII and NheI. GPX1 cDNA was cut using NheI and BamHI. The plasmid (pcDNA3.1) was cut with HindIII and BamHI. Finally, the three enzyme-digested fragments were ligated by T4 DNA ligase. The construction was confirmed by DNA sequencing.

Hyperinsulinemic-euglycemic clamp experiment

The hyperinsulinemic-euglycemic clamp experiment, the most widely used experimental procedure for the determination of insulin sensitivity, was performed as described previously (15). Briefly, food was withdrawn 12 h before the experiment. The rats were then anesthetized with amobarbital sodium (25 mg/kg, i.p.) and cannulated in the jugular vein for infusion of glucose and insulin (dual cannula) and in the carotid artery for sampling. All cannulae were tunneled subcutaneously and encased in silastic tubing (0.08 cm) sutured to the skin. After infusion of glucose (10%) and insulin (1 IU/mL) through dual cannula with constant velocity, the blood glucose levels were measured. To keep the blood sugar in a relatively steady state, the rate of glucose infusion was continuously adjusted. Glucose injection rate (GIR) was measured under homeostasis 6 times during the experiment.

Insulin sensitivity assay by short insulin tolerance test using capillary blood glucose

Insulin sensitivity assay was performed as described previously (15). Rats were weighed and placed into mouse cage after fasting overnight. Blood glucose was detected 6 times after i.p. administration of insulin (0.05 U/kg) using a blood sugar detector. The abscissa indicates time and the ordinate expresses the natural logarithm of blood sugar. The regression coefficient (r) or slope was determined by linear regression and K_{ITT} was calculated by multiplying r by 100. The K-value indicates insulin sensitivity with smaller K-values for lower sensitivities.

Western blotting

Immunoblotting was performed in thoracic aorta and

soleus to detect GPX1, p-eNOS, and eNOS protein levels as previously described (22). Briefly, the aorta and soleus of each rat were individually homogenized in 5 volumes of homogenization buffer containing 1 mM EDTA, 1 mM EGTA, 50 mM Tris–HCl (pH 7.5), 1 mM dithiothreitol (DTT), 5 mM sodium pyrophosphate, 10% glycerol, 1% Triton X-100, 0.1 mg/mL phenylmethylsulfonyl fluoride (PMSF), 50 mM NaF, and a protease inhibitor cocktail (Sigma). Homogenates were then centrifuged (10,000 × *g*) for 15 min at 4°C. Protein concentrations were assayed with the bicinchoninic acid (BCA) method (Pierce Biotechnology, Rockford, IL, USA), using bovine serum albumin (BSA) as the standard. Protein samples (45 μg) from aorta and soleus tissues or whole cell lysates of RAOECs were separated on 6% – 12% Tris-glycine gels and transferred to nitrocellulose membranes (Invitrogen). Membranes were then probed with antibodies against eNOS, phospho-eNOS, GPX1, actin, and MCP-1 followed by incubation with horseradish peroxidase–associated secondary antibodies before signals were visualized with the enhanced chemiluminescence detection system (Amersham Bioscience, Piscataway, NJ, USA).

eNOS activity assay

Endothelial NO synthase activity was measured as previously described (23, 24). Briefly, the thoracic aortas (35 mm) were isolated and cut longitudinally. The endothelial cells were removed using a scraper and then sonicated in a buffer (250 mM sucrose, 1 mM DTT, 50 mM Tris, 20 mM HEPES, 10 μg/mL leupeptin, 5 μg/mL aprotinin, 10 μg/mL soybean trypsin inhibitor, and 0.1 mM PMSF). After centrifugation and determination of protein concentration (BCA method), aliquots of 40 μL were added to 80 μL of a reaction buffer containing 1 mM NADPH, 50 mM Tris, 20 mM HEPES, 0.1 mM tetrahydrobiopterin, 50 μM FMN, 1 mM DTT, 50 μM FAD, and 8 μCi/mL L-2,3-[^{3}H]arginine (New England Nuclear, Boston, MA, USA) and incubated for 20 min at 37°C in the presence of 3 mM $CaCl_2$ and 10 μg/mL calmodulin or with 3 mM EGTA in absence of Ca^{2+}/calmodulin. The reaction was terminated by adding 1 mL of ice-cold distilled water. The mixture applied to an anion-exchange chromatography column containing Dowex AG 50W-X8 resin saturated with 50 mM Tris (2 mL) and 100 mM L-citrulline (50 μL), 20 mM HEPES buffer (pH 7.4) and eluted with 2 mL of distilled water. Concentration of the eluted L-[^{3}H]citrulline was detected with a liquid scintillation counter. The calcium-dependent NOS activity was calculated as the difference between activity in the presence and absence of Ca^{2+}/calmodulin. Values were corrected to the protein content in the homogenates and the incubation time (cpm per mg protein per min).

Measurement of reactive oxygen species (ROS)

To detect the intracellular ROS generation, the fluorescent indicator 2′,7′-dihydrodichlorofluorescin diacetate (DCFDA, Molecular Probes, Eugene, OR, USA) was employed in endothelial cells (ECs) as described previously (25). The confluent ECs in 96-well plates were preincubated with DCFDA (10 μM) for 30 min. Cells were washed three times in PBS, followed by measurement of fluorescence intensity at 485-nm excitation and 538-nm emission spectra using a microplate reader (Wallac 1420 VICTOR2; PerkinElmer, Waltham, MA, USA). The ROS formation in rat aorta and skeletal muscle (soleus) was determined as described previously (26, 27). These procedures were performed in dark conditions to avoid photo-oxidation. Data are presented as the fold increase in DCF fluorescence compared with that in unstimulated cells, aorta, or muscle tissues.

Measurement of NO production

NO quantification was performed using the NO-specific fluorescent dye 4,5-diaminofluorescein diacetate (DAF-2 DA; Cayman Chemical, Ann Arbor, MI, USA) as described previously (28). Briefly, ECs were seeded in 96 well-plates (3×10^4 cells/well), cultured for 24 h, and treated with 0.3 mM palmitate for 24 h in the presence or absence of GPX1 transfection, PEG-catalase (500 U/mL), or tranilast (200 μM). The cells were then serum-starved for 1 h in phenol red-free EBM supplemented with L-arginine (100 μM). Cells were then loaded with DAF-2DA (5 μM final concentration) for 10 min at 37°C. After being loaded with DAF-2 DA, cells were washed three times with EBM at 37°C and kept in the dark. The fluorescence intensity was measured with a multilabel plate reader (485 nm excitation, 535 nm emission). The fluorescence intensities were corrected by subtracting the non-specific fluorescence in wells without addition of DAF-2 DA and in wells without cells. The endothelial NO production in aortas was measured by electron spin resonance (ESR) as described previously (29). Results are expressed as relative intensity units per milligram of tissue.

Reverse transcription polymerase chain reaction (RT-PCR) and real-time quantitative RT-PCR (qRT-PCR)

Total RNA from aortic segments (approximately 25 mg) or RAOECs was extracted using TRIzol reagent (Sigma), and RT-PCR was performed using the SuperScript One-Step RT-PCR kit (Invitrogen) according to manufacturer's protocol to determine GPX1 mRNA expression. qRT-PCR using a pair of hybridization probes to detect the target and the reference amplicon of the aortic or RAOEC RNA extract was used to quantify GPX1 mRNA expression. GAPDH mRNA, the expression of

which is independent of dietary fat composition (30), was used as a housekeeping control to correct for sample inhomogeneity. qRT-PCR was performed in a 96 well format in the Bio-Rad CFX96 Real Time System (Bio-Rad Laboratories, Hercules, CA, USA). In each reaction, 150 – 300 ng RNA from the aorta was added and the $MgCl_2$ concentration was adjusted to 6 mM. The rat GPX1 primers were 5′-CATCAGGAGAATGGC AAGAA-3′ and 5′-TCACCTCGCACTTCTCAAAC-3′. The rat GAPDH primers were 5′-TCCCTCCAGATT GTCAGCAA-3′ and 5′-AGATCCACAACGGATACA TT-3′. After 30 min at 55°C for transcription, there were 45 rounds of amplification at 90°C (5 s), 64°C (15 s), and 72°C (15 s). Melting curves were used to validate product specificity. All samples were amplified in triplicate from the same total RNA preparation and the mean value was used for further analysis.

Statistical analyses

All data are given as the mean ± S.D.; n is the number of rats. Western blot and q-RT-PCR analysis data are expressed relative to the control, assigning a value of 1 to the control group baseline mean. Data were analyzed using Student's *t*-test or 2-way ANOVA as appropriate. A *P*-value of < 0.05 was taken as a significant difference between data sets.

Results

Body mass and metabolic changes

Table 1 shows that treatment with tranilast during chronic ingestion for 4 weeks of the HFE significantly attenuated the increases in final body weight and drinking amount when compared with the untreated HFE-fed rats, although they remained significantly heavier than the controls. In addition, tranilast significantly blocked the increases in visceral fat induced by HFE. Further-

Table 1. Body weight, average daily food intakes, drinking, and visceral fat of Wistar rats that received either common water (control) or a high-fat emulsion (HFE) for 4 weeks, with or without tranilast treatment

	Control	Tranilast	HFE	HFE + tranilast
Body weight (g)	212.6 ± 17.8	210.4 ± 16.9	240.5 ± 18.6*	226.7 ± 16.3*,#
Food intake (g/day)	80.2 ± 5.4	82.5 ± 6.2	76.6 ± 6.8	78.8 ± 5.8
Drink (mL)	146.2 ± 15.3	149.3 ± 16.6	238.5 ± 22.6*	176.8 ± 18.7*,#
Visceral fat (g)	9.8 ± 4.5	9.3 ± 4.2	15.9 ± 5.8*	11.7 ± 4.8#

Values are the mean ± S.D. n = 15; *$P < 0.05$, compared with the control group; #$P < 0.05$, compared with the HFE group.

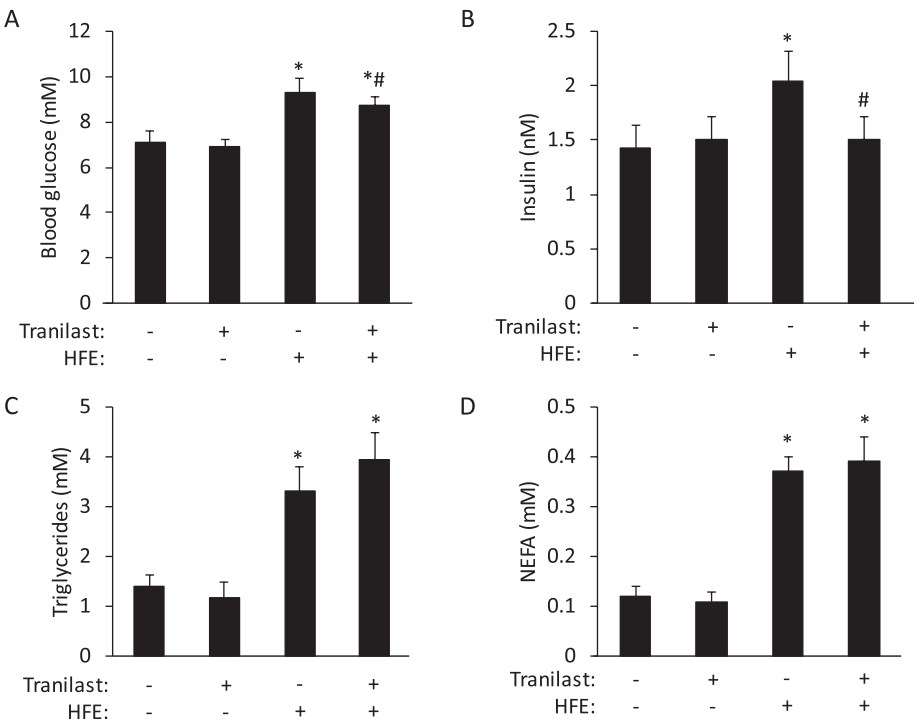

Fig. 1. Plasma levels of glucose, insulin, triglycerides, and nonesterified fatty acids (NEFA) measured in Wistar rats that received either water (control) or a high-fat emulsion (HFE) for 4 weeks, with or without tranilast treatment. HFE: high-fat emulsion group. Values are the mean ± S.D., n = 9. *$P < 0.05$, compared with the control group; #$P < 0.05$, compared with the HFE group.

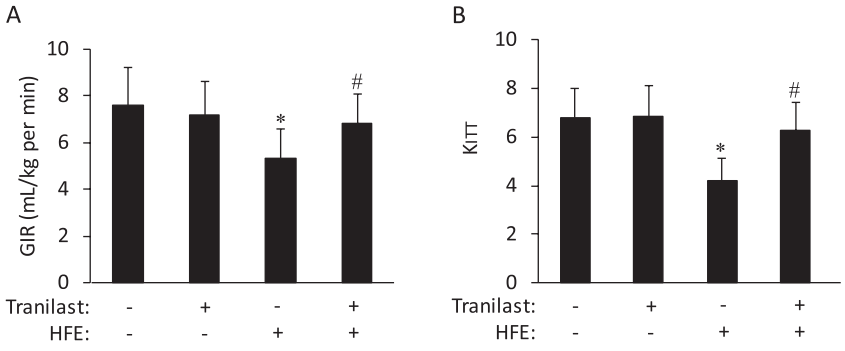

Fig. 2. Results of insulin sensitivity assay in the hyperinsulinemic-euglycemic clamp test (A) and changes of glucose induced by insulin injection (B). GIR: glucose injection rate; K_{ITT}: glucose disappearance rate. Values are the mean ± S.D., n = 8. $^{*}P < 0.05$, compared with the control group; $^{\#}P < 0.05$, compared with the HFE group.

more, tranilast treatment completely prevented the increase elicited by the HFE diet in plasma insulin levels; a moderate but significant reduction in glucose plasma levels was noted in tranilast-treated HFE-fed rats when compared to the untreated HFE-fed rats (Fig. 1: A and B). The higher plasma triglycerides and NEFA levels noted in HFE-fed rats, when compared to the control rats, were not altered by the treatment with tranilast (Fig. 1: C and D). Table 1 and Fig. 1 indicate that treatment with tranilast had no significant effect on various biological parameters measured in the non-HFE-treated groups.

Tranilast reduces high-fat diet–induced insulin resistance

Our hyperinsulinemic-euglycemic clamp test indicated that the GIR for keeping homeostasis of blood glucose in rats of HFE group was decreased versus the control (Fig. 2A), suggesting that the HFE diet induced insulin resistance in rats. Tranilast treatment significantly restored GIR in HFE-fed rats. Furthermore, the results of th short insulin tolerance test using capillary blood glucose revealed that K_{ITT} decreased to 4.1 ± 0.7 in rats treated with fat emulsion (i.g., 4 w) ($P < 0.05$, n = 8). Tranilast treatment significantly blocked this decrease in HFE-fed rats (Fig. 2B). Together, our results demonstrate that tranilast reduces high-fat diet–induced insulin resistance in Wistar rats.

Tranilast enhances endothelium-dependent vasorelaxation in HFE-fed rat aortas

To determine whether tranilast treatment modulates the endothelial function in the dietary model of insulin resistance, we investigated the vascular response to endothelium-dependent and -independent vasodilators and the influence of endothelium on the response to vasoconstrictors in vessel rings. Using this method, we found that the vasoconstrictor responses to phenylephrine were not significantly altered by the HFE diet, nor by treatment with tranilast (Fig. 3A). However, the endothelium-dependent relaxation induced by increasing concentrations of carbachol was significantly lower in aortic rings from HFE-fed rats than those from the control group (Fig. 3B). Tranilast treatment in HFE-fed rats completely prevented the reduction in the vasorelaxing responses to carbachol. However, tranilast treatment had no effect on the vascular response to carbachol in the control rats. The endothelium-independent vasorelaxation to SNP revealed that vascular smooth muscles from the 4 groups of rats had a similar ability to relax (Fig. 3C). These results suggest that tranilast alleviates endothelial dysfunction (i.e., decreased endothelium-dependent vasorelaxation) in HFE-fed rats.

Tranilast prevents oxidative damage and inflammation via protecting GPX1 in HFE-fed rats

To investigate the mechanism by which tranilast ameliorates endothelial dysfunction and insulin resistance induced by high-fat diet, we measured the levels of glutathione peroxidase-1 (GPX1) and ROS formation. GPX1 is a crucial antioxidant enzyme, the deficiency of which promotes atherogenesis (31). As indicated in Fig. 4A, tranilast treatment was found to prevent the reduction in GPX1 mRNA expression seen in aortas isolated from untreated HFE-fed rats. More importantly, tranilast treatment during chronic ingestion of the HFE diet significantly prevented the decreases in GPX1 protein expression and increase in H_2O_2 formation in both vascular and skeletal muscle tissues (Fig. 4: B and C). Indeed, these respective levels of expression noted in the thoracic aorta and soleus isolated from tranilast-treated normal-diet rats were not different from those measured in control rats. Since ROS mediates the inflammatory pathways that participate in the development and progression of atherosclerosis (32), we examined aortic monocyte chemoattractant peptide-1 (MCP-1), which is one of the earliest molecular markers of vascular inflammation in atherogenesis (33). MCP-1 levels were significantly increased in the aortas of HFE-fed rats compared with control rats and this increase was dramatically inhibited by tranilast treatment (Fig. 4D).

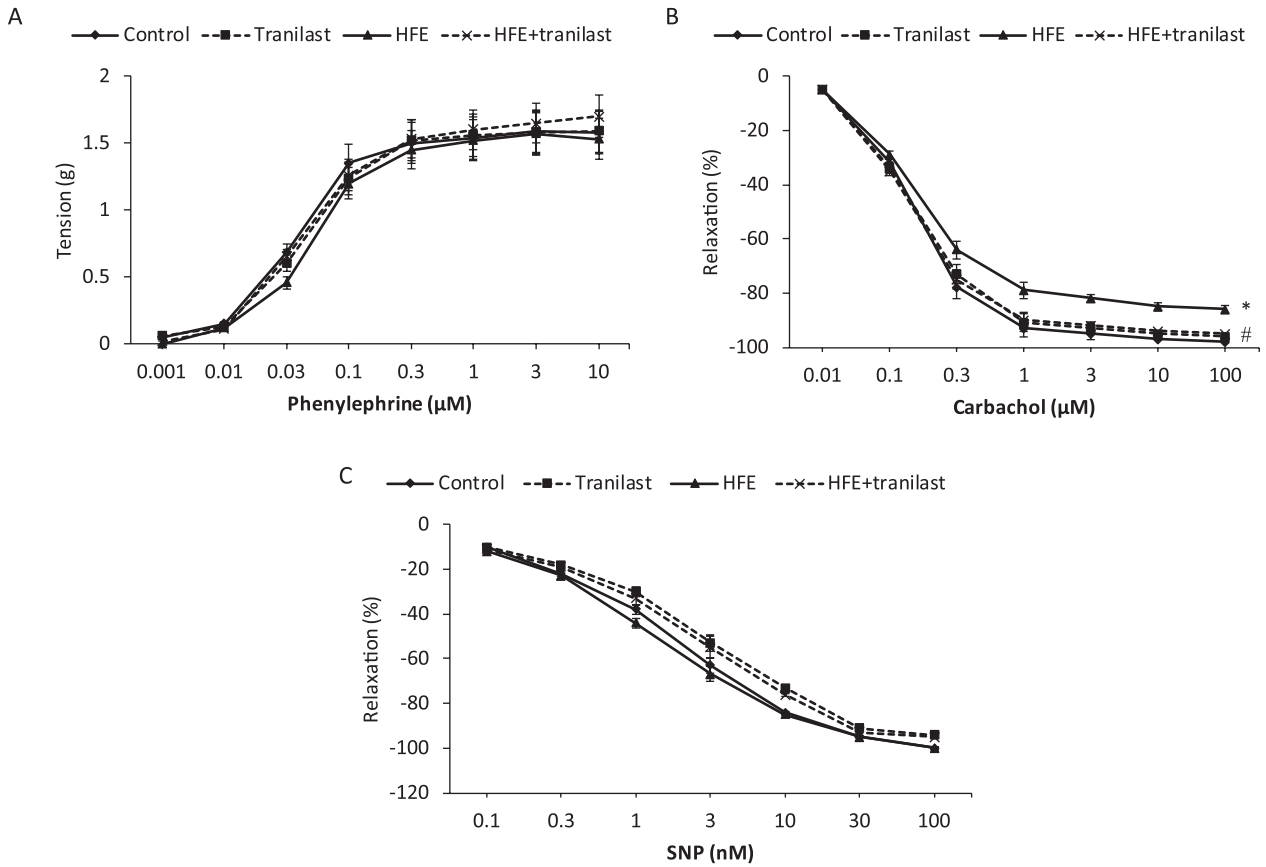

Fig. 3. Cumulative dose–response curves to phenylephrine (A) in isolated aortic rings from Wistar rats (n = 15). Developed tensions are expressed in grams, and values are the mean ± S.D. Data were analyzed using a 2-way repeated-measures ANOVA, and post-hoc analyses were performed (Fisher's exact test) when appropriate. Cumulative dose–response curves to carbachol (B) or sodium nitroprusside (SNP) (C) in isolated aortic rings from Wistar rats (n = 15). The aortic rings were precontracted with phenylephrine. Relaxations are expressed as percent changes from the initial precontraction induced by phenylephrine, and values are the mean ± S.D. Data were analyzed using a 2-way repeated measures ANOVA, and post-hoc analyses were performed (Fisher's exact test) when appropriate; $^{*}P < 0.05$, for the HFE-fed compared with the control group; $^{\#}P < 0.05$, for the HFE-fed tranilast-treated group compared with the HFE-fed group.

Our results suggest that tranilast shows a significant anti-oxidant and anti-inflammatory effect in vivo.

Tranilast blocks HFE-induced decrease in eNOS activity and NO bioavailability

The endothelial isoform of NOS (eNOS)-derived NO bioactivity is the most important for the maintenance of vascular homeostasis (34). To further elucidate the mechanism by which tranilast prevents endothelial dysfunction induced by HFE, we investigated eNOS phosphorylation, activity, and NO production in the thoracic aorta isolated from overnight-fasted control, tranilast-treated, HFE-fed, and tranilast-treated HFE-fed Wistar rats. As shown in Fig. 5, eNOS phosphorylation at Ser1177, which represents an important mechanism of eNOS activation; eNOS activity; and NO production were significantly lower in the thoracic aorta from HFE-fed rats than from control rats. Tranilast treatment significantly prevented the reduction in eNOS activity and NO release elicited by the HFE diet. Indeed, the eNOS protein expressions were not different between these 4 groups. Our results suggest that tranilast protects endothelial function probably via blocking HFE-induced decrease in eNOS activity and NO bioavailability.

Tranilast protects eNOS activity and NO bioavailability against FFA-induced oxidative damage via preserving GPX1 expression

To further substantiate the molecular mechanism underlying the endothelial protecting effect of tranilast, we employed in vitro studies by using cultured RAOECs treated with palmitic acid (PA), the most abundant fatty acids in western diets, and tranilast. First, to investigate the role of GPX1 in PA-induced damage in ECs, we

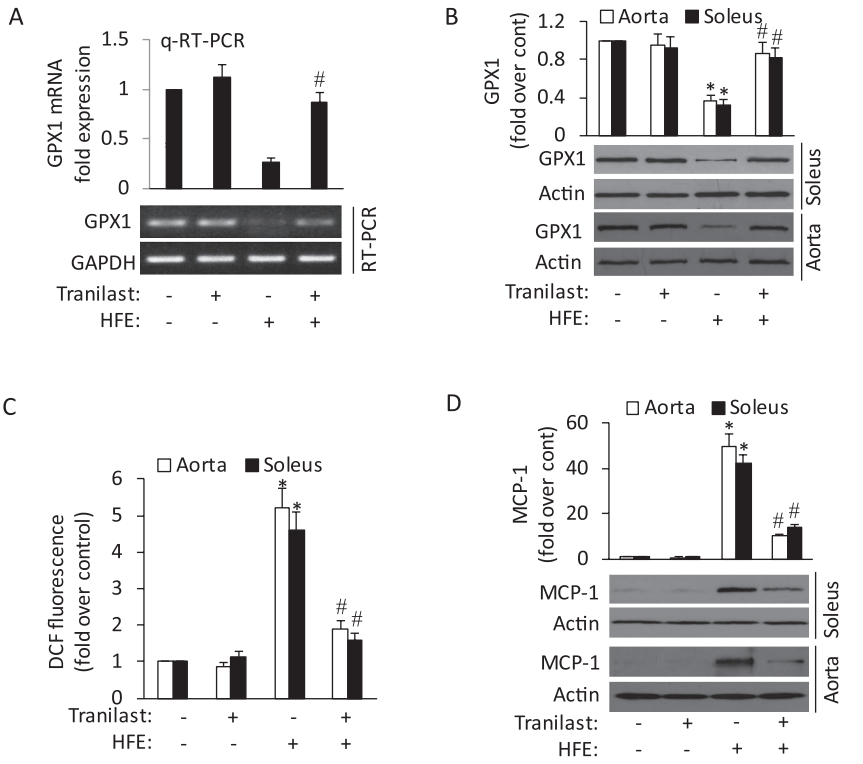

Fig. 4. Effects of a high-fat emulsion diet (HFE) and tranilast treatment on GPX1 expression, ROS formation, and MCP-1 expression in the vascular or muscle tissues. Representative real-time quantitative RT-PCR (upper panel), RT-PCR (lower panel) (A), and western blot (B) depicting GPX1 mRNA and protein expression in the thoracic aorta or soleus isolated from overnight-fasted control, tranilast-treated, HFE-fed, and tranilast-treated HFE-fed (n = 8) Wistar rats. The mean level of GPX1 in control rats was assigned a value of 1, and the relative values are expressed as fold induction over the control group. C: Intracellular ROS was assessed by fluorescence intensity of dichlorofluorescin (DCF fluorescence) emission. Data are presented as mean fold increases (± S.D.) in treated groups over basal values from 4 independent experiments. D: Representative western blot (lower panel) and group data (upper panel) depicting MCP-1 expression in the thoracic aorta or soleus isolated from overnight-fasted control, tranilast-treated, HFE-fed, and tranilast-treated HFE-fed (n = 8) Wistar rats. Data are expressed as the mean ± S.D. and were analyzed using unpaired Student's *t*-tests; $^{*}P < 0.05$, compared with the control rats; $^{\#}P < 0.05$, compared with the HFE-fed rats.

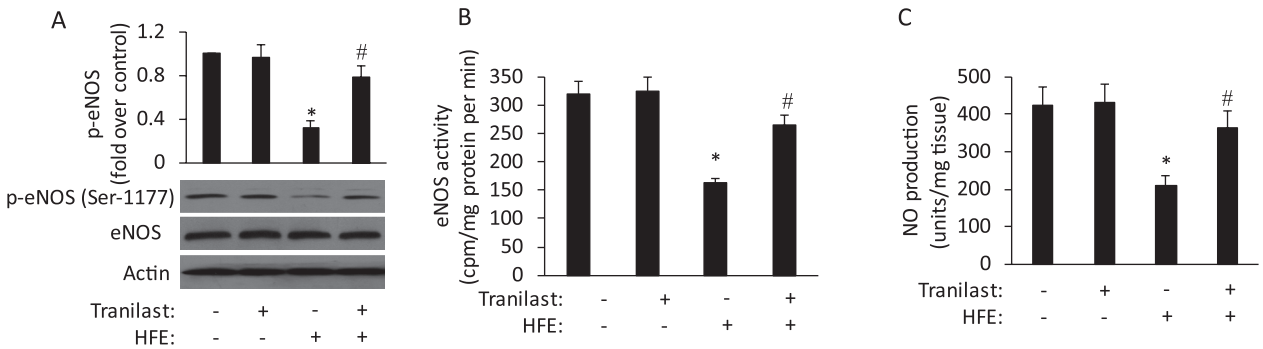

Fig. 5. Effects of a high-fat emulsion diet (HFE) and tranilast treatment on p-eNOS levels, eNOS expression and activity, and NO production in the vascular tissues. A: Representative western blot (lower panel) and group data (upper panel) depicting p-eNOS levels in the thoracic aorta isolated from overnight-fasted control, tranilast-treated, HFE-fed, and tranilast-treated HFE-fed (n = 8) Wistar rats. B: Activity levels of eNOS, expressed as cpm per milligram of protein in aortic endothelial lining from control, tranilast-treated, HFE-fed, and tranilast-treated HFE-fed (n = 8) Wistar rats. C: NO production by aortic segments from rats fed a HFE with or without tranilast treatment evaluated by ESR of the DETC-Fe-NO complex (n = 6). Data are expressed as the mean ± S.D. and were analyzed using unpaired Student's *t*-tests; $^{*}P < 0.05$, compared with the control rats; $^{\#}P < 0.05$, compared with the HFE-fed rats.

treated RAOECs with 0.3 mM PA for various times and assessed GPX1 protein and mRNA levels. In addition, the protein and phosphorylation levels of eNOS, were also detected. As shown in Fig. 6, A and B, prolonged incubation (12 – 48 h) of RAOECs with 0.3 mM PA caused significant decreases in GPX1 protein and mRNA levels as well as phosphorylated eNOS levels. To ensure reduced GPX1 levels indeed play a role in PA-induced eNOS inhibition, we showed that GPX1 overexpression significantly rescued PA-induced phospho-eNOS reduction and ROS formation (Fig. 6: C and D). In addition, to further substantiate PA-induced eNOS inhibition and compromised NO production were attributed to ROS accumulation, ECs were treated with PA for 24 h in the presence of PEG-catalase, a potent H_2O_2 scavenger. As shown in Fig. 6, C and D, PEG-

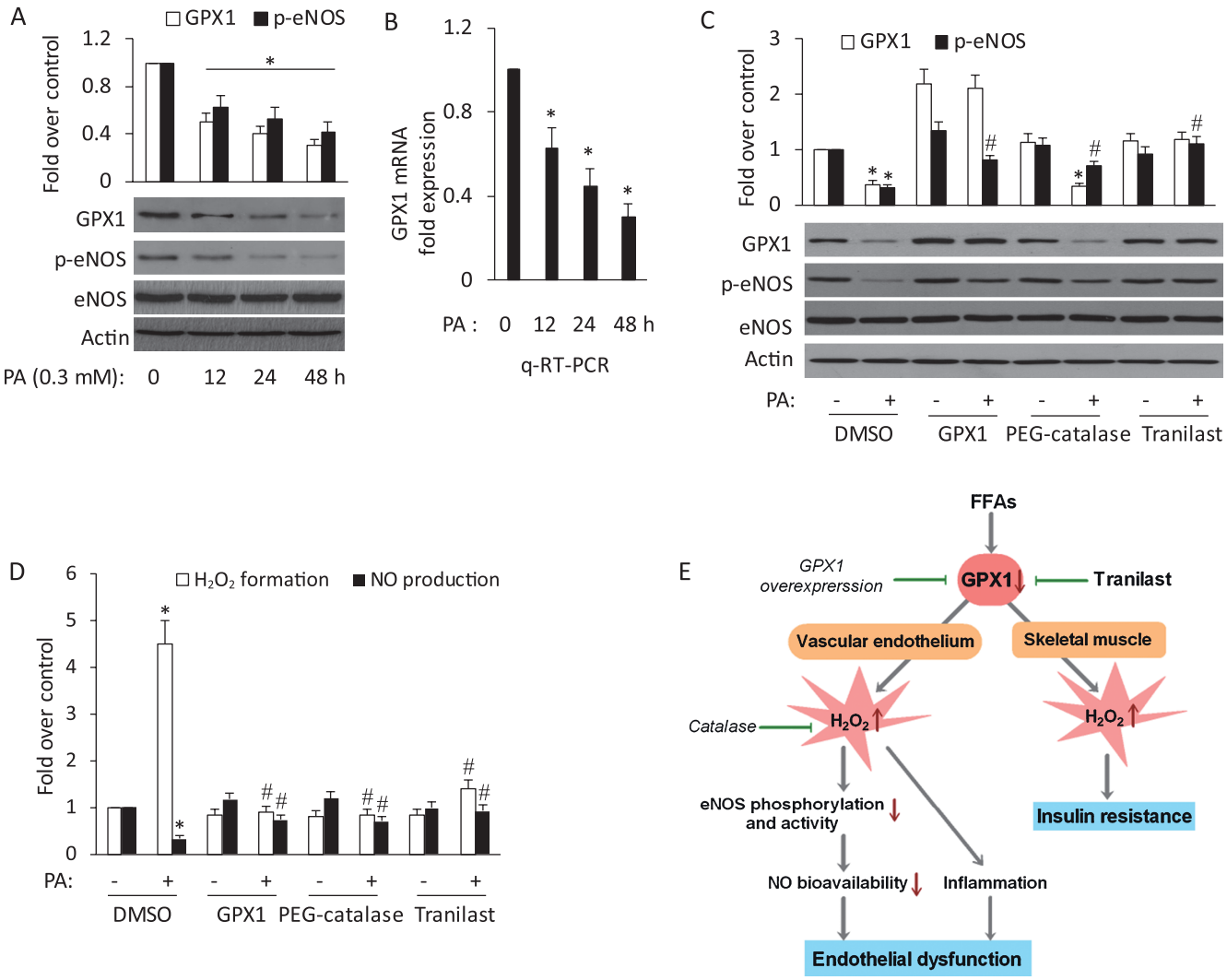

Fig. 6. Tranilast blocks palmitic acid-induced eNOS inhibition and NO bioavailability decrease via protecting antioxidant enzyme GPX1. A: RAOECs were incubated with 0.3 mM palmitic acid (PA) for 0 – 48 h before protein and phosphorylation analyses. The blots are representative of 3 individual experiments (n = 3). *$P < 0.05$ vs. control. B: GPX1 mRNA expression in endothelial cells was assessed by q-RT–PCR. Each bar represents mean ± S.D. of 3 independent assays. C: ECs were treated with PA (0.3 mM) or its vehicle BSA for 24 h in the presence or absence of GPX1 expression vector transfection, PEG-catalase (500 U/mL) or tranilast (200 μM) or its solvent (0.05% DMSO). GPX1 protein levels were confirmed by immunoblotting. The cells lysates were analyzed by immunoblotting using anti-GPX1 antibody, anti-phospho-serine 1177 eNOS polyclonal antibody (p-eNOS), or eNOS antibody. D: H_2O_2 formation and NO production were measured as described in "Materials and Methods". *$P < 0.05$ vs. their corresponding controls; $^{\#}P < 0.05$ vs. PA-treated group. E: The proposed mechanism by which tranilast inhibits the oxidative damage and pro-inflammatory effects of FFA. FFA suppresses GPX1 protein expression, which is critical for its activity, and consequent induction of ROS with resultant eNOS inhibition, decreased NO bioavailability, and inflammation in the endothelium. Tranilast suppresses ROS formation by rescuing GPX1 expression. Overall, we consider tranilast protects anti-oxidant enzymes such as GPX1 to suppress endothelial oxidative damage.

catalase significantly blocked PA inhibition of eNOS and NO production. More importantly, tranilast preserved GPX1 expression in PA-treated ECs with a consequent decreased ROS formation and increased eNOS phosphorylation and NO production. Taken together, in the present study, we demonstrate that tranilast protects eNOS activity and NO bioavailability against FFA-induced oxidative damage via preserving antioxidant enzyme GPX1 expression in endothelial cells (Fig. 6E).

Discussion

We demonstrate that several alterations induced by a HFE diet in rats can be attenuated or prevented by

tranilast treatment. First, a significant reduction in body mass gain and visceral fat accretion were noted, and a marked improvement in insulin sensitivity was observed in tranilast-treated HFE-fed rats. Secondly, tranilast treatment prevented the increases in plasma glucose and insulin levels, as well as the alterations in vascular responses to the endothelium-dependent vasodilator carbachol. These improvements were associated with higher levels of GPX1 and marked reductions in H_2O_2 formation and MCP-1 expression (an inflammation marker) in vascular endothelium and skeletal muscle. These results suggest that both oxidative stress and inflammation processes causing detrimental effects on vascular endothelium and skeletal muscle could play a pivotal role in the early vascular and metabolic changes induced by consumption of an obesity-inducing diet. This is consistent with previous reports indicating that macronutrient intake can induce oxidative stress and inflammatory responses that could damage vascular integrity over time and cause endothelial dysfunction (35 – 37). Our results suggest that an early intervention aiming to control one of these initiating factors, oxidative stress, might attenuate, or even prevent the pathophysiological processes leading to the development of chronic diseases. Intriguingly, tranilast treatment did not appear to have any significant effect on the cardiovascular responses or the other metabolic parameters measured in control rats.

Four weeks of tranilast treatment prevented the deleterious effects of HFE diet on vascular responses. The vascular responses noted in tranilast-treated HFE-fed rats were not different from those seen in the control group. Tranilast treatment was found to prevent the reduction in eNOS phosphorylation and activity and NO production in vascular tissues of HFE-fed rats, suggesting a prominent role for ROS in the reduced eNOS activity and NO bioavailability. These findings are further supported by the demonstration here that lowering oxidant stress in HFE-fed rats improves the vasorelaxing responses of carbachol. In contrast, the endothelium-independent vasorelaxations to SNP were similar in the 4 experimental groups, indicating that the ability of vascular smooth muscle to relax, in response to exogenous NO, was not altered by the HFE diet or the treatment with tranilast. In addition, in vitro studies demonstrated that GPX1 overexpression or PEG-catalase, a potent H_2O_2 scavenger, significantly rescued FFA-induced ROS formation and phospho-eNOS reduction (Fig. 6: C and D). More importantly, tranilast preserved GPX1 expression in FFA-treated ECs with a consequent decreased ROS formation and increased eNOS phosphorylation and NO production. Therefore, the mechanisms underlying the ability of tranilast to prevent endothelial dysfunction could involve an inhibition in ROS production, as well as an enhanced NO bioactivity, both leading to an improvement in endothelium-dependant vascular responses. Indeed, H_2O_2 oxidizes tetrahydrobiopterin (BH4) to dihydrobiopterin, which is an ineffective cofactor for NOS-dependent NO generation (38), and downregulates tetrahydrobiopterin (BH4) salvage enzyme dihydrofolate reductase (DHFR) and DHFR/eNOS ratio, leading to BH4 deficiency and subsequently uncoupling of eNOS (39). Thus, tranilast treatment, via inhibiting H_2O_2 accumulation, might have enhanced eNOS activity and NO production by preventing the uncoupling of vascular eNOS and restoring its synthesis of NO rather than $O2^{-}$.

The whole-body insulin sensitivity index measured in tranilast-treated HFE-fed rats was significantly higher than that measured in the untreated HFE-fed group. More and more evidence has suggested that ROS, including H_2O_2, functions as signaling molecules involved in the regulation of cellular function. The increased production of these reactive molecules or an impaired capacity for their elimination, also termed oxidative stress, result in abnormal changes in intracellular signaling and lead to chronic inflammation and insulin resistance. Previous studies suggest that oxidative stress and inflammation have been linked to insulin resistance in vivo (40). Skeletal muscle is the predominant site of insulin-mediated glucose uptake in the postprandial state. Under euglycemic hyperinsulinemic conditions, approximately 80% of glucose uptake occurs in skeletal muscle (41). Previous studies suggest that the defect in insulin action in the skeletal muscle is the main cause of type 2 diabetes (42 – 44). In the present study, given that tranilast preserves antioxidant enzyme GPX1 and suppresses oxidative stress in skeletal muscle (Fig. 4), we believe that tranilast, via decreasing oxidative stress in skeletal muscle, alleviates whole-body insulin resistance in high-fat diet–fed rats. On the other hand, in agreement with previous studies showing evidence of an NO-dependent mechanism that modulates peripheral insulin action (45, 46), we cannot exclude the possibility that, besides the antioxidative effect, the improvement in insulin sensitivity noted in tranilast-treated rats involves a mechanism that is dependent on tranilast-induced protective effect on NO bioavailability. In other words, the preventative effect of tranilast on ROS production and NO breakdown may have attenuated insulin resistance by improving vascular responses to insulin, and possibly, by enhancing skeletal muscle microperfusion preferentially to areas with high rates of glucose uptake, as shown by others in healthy rats (47, 48).

Tranilast reduced body mass gain and visceral fat accretion and improved insulin sensitivity in the HFE-

fed rats. Two mechanisms can be used to explain weight gain loss with tranilast treatment. Insulin is a very anabolic hormone. In addition to its main physiological role of inhibiting hepatic glucose output and stimulating peripheral glucose uptake, insulin also stimulates the uptake of amino acids and has equally important roles on free fatty acid metabolism (inhibiting lipolysis and promoting lipogenesis) and protein metabolism, contributing to its overall anabolic effect (49). Thus, increased insulin levels or insulin therapy commonly results in weight gain in both type 2 and type 1 diabetes (49). It is well known that the strategy that can be expected to limit weight gain in the case of increased insulin or insulin therapy is to increase the patient's insulin sensitivity, which can limit the required insulin dose or decrease insulin secretion. For example, metformin is an important pharmacological intervention to increase insulin sensitivity and it has been associated with weight loss in type 2 diabetes and with insulin-sparing and cardioprotective properties (50, 51). In addition, metformin can also be used to limit weight gain in patients beginning insulin therapy (52). Accordingly, by improving insulin sensitivity in the HFE-fed rats, tranilast significantly decreases plasma insulin levels (Fig. 1B). This action can explain weight gain loss with tranilast treatment. The other mechanism underlying the weight-sparing properties of tranilast may relate to oxidative stress suppression. Previous studies (53 – 55) found that body mass index (BMI) and waist circumference (WC) in healthy middle-aged women and obesity subjects are positively correlated with systemic oxidative stress. In contrast, parameters of antioxidant capacity are inversely related to the amount of body fat and central obesity (56, 57). Furthermore, weight gain induced by high-fat feeding involves increased liver oxidative stress (58). In the present study, the anti-oxidant property of tranilast may contribute to its weight-sparing effect.

Excessive consumption of high-saturated-fat food is considered among the most important environmental factors leading to an increase in the prevalence of metabolic syndrome, a leading cause of atherosclerotic cardiovascular disease (CVD). Oxidative stress, low-grade inflammation, and endothelial dysfunction, were reported in various populations at risk for metabolic syndrome and CVD and could play a key role in the pathophysiology of the vasculopathy associated with the disease (37, 59 – 61). The present study, using a short-term dietary intervention and a preventive treatment with tranilast in an animal model suggests that an early intervention aiming to control one of these initiating factors, oxidative stress, may prevent "the early start of a dangerous situation" (60) that could cause the development of long-term and irreversible vascular and metabolic complications. In conclusion, tranilast is worthy of further investigation as a drug that may be therapeutically useful in the inhibition of atherosclerotic development.

Conflicts of Interest

The authors report no conflicts of interest.

References

1 McGovern PG, Pankow JS, Shahar E, Doliszny KM, Folsom AR, Blackburn H, et al. Recent trends in acute coronary heart disease--mortality, morbidity, medical care, and risk factors. The Minnesota Heart Survey Investigators. N Engl J Med. 1996;334:884–890.

2 Davidson SM, Duchen MR. Endothelial mitochondria: contributing to vascular function and disease. Circ Res. 2007;100:1128–1141.

3 Deedwania PC. Endothelium: a new target for cardiovascular therapeutics. J Am Coll Cardiol. 2000;35:67–70.

4 Ross R. Atherosclerosis--an inflammatory disease. N Engl J Med. 1999;340:115–126.

5 Mano T, Masuyama T, Yamamoto K, Naito J, Kondo H, Nagano R, et al. Endothelial dysfunction in the early stage of atherosclerosis precedes appearance of intimal lesions assessable with intravascular ultrasound. Am Heart J. 1996;131:231–238.

6 Tooke JE. Microvascular function in human diabetes. A physiological perspective. Diabetes. 1995;44:721–726.

7 Namazi MR, Soma J. Tranilast: a novel weapon against insulin resistance. Med Hypotheses. 2005;64:1135–1137.

8 Matsumura T, Kugiyama K, Sugiyama S, Ota Y, Doi H, Ogata N, et al. Suppression of atherosclerotic development in Watanabe heritable hyperlipidemic rabbits treated with an oral antiallergic drug, tranilast. Circulation. 1999;99:919–924.

9 Saiura A, Sata M, Hirata Y, Nagai R, Makuuchi M. Tranilast inhibits transplant-associated coronary arteriosclerosis in a murine model of cardiac transplantation. Eur J Pharmacol. 2001;433:163–168.

10 Stocker R, Keaney JF Jr. Role of oxidative modifications in atherosclerosis. Physiol Rev. 2004;84:1381–1478.

11 Madamanchi NR, Runge MS. Mitochondrial dysfunction in atherosclerosis. Circ Res. 2007;100:460–473.

12 Flohe L. Glutathione peroxidase. Basic Life Sci. 1988;49:663–668.

13 Forgione MA, Cap A, Liao R, Moldovan NI, Eberhardt RT, Lim CC, et al. Heterozygous cellular glutathione peroxidase deficiency in the mouse: abnormalities in vascular and cardiac function and structure. Circulation. 2002;106:1154–1158.

14 Forgione MA, Weiss N, Heydrick S, Cap A, Klings ES, Bierl C, et al. Cellular glutathione peroxidase deficiency and endothelial dysfunction. Am J Physiol Heart Circ Physiol. 2002;282:H1255–H1261.

15 Ai J, Wang N, Yang M, Du ZM, Zhang YC, Yang BF. Development of Wistar rat model of insulin resistance. World J Gastroenterol. 2005;11:3675–3679.

16 Richterich R, Kuffer H, Lorenz E, Colombo JP. [The determination of glucose in plasma and serum (hexokinase-glucose-6-phosphate dehydrogenase method) with the Greiner electronic selective analyzer GSA II (author's transl)]. Z Klin Chem Klin

Biochem. 1974;12:5–13. (text in German)
17 Desbuquois B, Aurbach GD. Use of polyethylene glycol to separate free and antibody-bound peptide hormones in radioimmunoassays. J Clin Endocrinol Metab. 1971;33:732–738.
18 Kohlmeier M. Direct enzymic measurement of glycerides in serum and in lipoprotein fractions. Clin Chem. 1986;32:63–66.
19 Christon R, Marette A, Badeau M, Bourgoin F, Melancon S, Bachelard H. Fatty acid-induced changes in vascular reactivity in healthy adult rats. Metabolism. 2005;54:1600–1609.
20 Bourgoin F, Bachelard H, Badeau M, Lariviere R, Nadeau A, Pitre M. Effects of tempol on endothelial and vascular dysfunctions and insulin resistance induced by a high-fat high-sucrose diet in the rat. Can J Physiol Pharmacol. 2013;91:547–561.
21 Ishida K, Morino T, Takagi K, Sukenaga Y. Nucleotide sequence of a human gene for glutathione peroxidase. Nucleic Acids Res. 1987;15:10051.
22 Bourgoin F, Bachelard H, Badeau M, Melancon S, Pitre M, Lariviere R, et al. Endothelial and vascular dysfunctions and insulin resistance in rats fed a high-fat, high-sucrose diet. Am J Physiol Heart Circ Physiol. 2008;295:H1044–H1055.
23 Miatello R, Risler N, Castro C, Gonzalez S, Ruttler M, Cruzado M. Aortic smooth muscle cell proliferation and endothelial nitric oxide synthase activity in fructose-fed rats. Am J Hypertens. 2001;14:1135–1141.
24 Shinozaki K, Kashiwagi A, Nishio Y, Okamura T, Yoshida Y, Masada M, et al. Abnormal biopterin metabolism is a major cause of impaired endothelium-dependent relaxation through nitric oxide/O2- imbalance in insulin-resistant rat aorta. Diabetes. 1999;48:2437–2445.
25 Wang L, Sapuri-Butti AR, Aung HH, Parikh AN, Rutledge JC. Triglyceride-rich lipoprotein lipolysis increases aggregation of endothelial cell membrane microdomains and produces reactive oxygen species. Am J Physiol Heart Circ Physiol. 2008;295:H237–H244.
26 Korystov YN, Emel'yanov MO, Korystova AF, Levitman MK, Shaposhnikova VV. Determination of reactive oxygen and nitrogen species in rat aorta using the dichlorofluorescein assay. Free Radic Res. 2009;43:149–155.
27 Merry TL, Steinberg GR, Lynch GS, McConell GK. Skeletal muscle glucose uptake during contraction is regulated by nitric oxide and ROS independently of AMPK. Am J Physiol Endocrinol Metab. 2010;298:E577–E585.
28 Formoso G, Chen H, Kim JA, Montagnani M, Consoli A, Quon MJ. Dehydroepiandrosterone mimics acute actions of insulin to stimulate production of both nitric oxide and endothelin 1 via distinct phosphatidylinositol 3-kinase- and mitogen-activated protein kinase-dependent pathways in vascular endothelium. Mol Endocrinol. 2006;20:1153–1163.
29 Lopez D, Orta X, Casos K, Saiz MP, Puig-Parellada P, Farriol M, et al. Upregulation of endothelial nitric oxide synthase in rat aorta after ingestion of fish oil-rich diet. Am J Physiol Heart Circ Physiol. 2004;287:H567–H572.
30 Troyer DA, Chandrasekar B, Barnes JL, Fernandes G. Calorie restriction decreases platelet-derived growth factor (PDGF)-A and thrombin receptor mRNA expression in autoimmune murine lupus nephritis. Clin Exp Immunol. 1997;108:58–62.
31 Lubos E, Kelly NJ, Oldebeken SR, Leopold JA, Zhang YY, Loscalzo J, et al. Glutathione peroxidase-1 deficiency augments proinflammatory cytokine-induced redox signaling and human endothelial cell activation. J Biol Chem. 2011;286:35407–35417.
32 Guevara-Patino A, Sandoval de Mora M, Farreras A, Rivera-Olivero I, Fermin D, de Waard JH. Soft tissue infection due to Mycobacterium fortuitum following acupuncture: a case report and review of the literature. J Infect Dev Ctries. 2010;4:521–525.
33 Piga R, Naito Y, Kokura S, Handa O, Yoshikawa T. Short-term high glucose exposure induces monocyte-endothelial cells adhesion and transmigration by increasing VCAM-1 and MCP-1 expression in human aortic endothelial cells. Atherosclerosis. 2007;193:328–334.
34 Palmer RM, Ferrige AG, Moncada S. Nitric oxide release accounts for the biological activity of endothelium-derived relaxing factor. Nature. 1987;327:524–526.
35 Mohanty P, Ghanim H, Hamouda W, Aljada A, Garg R, Dandona P. Both lipid and protein intakes stimulate increased generation of reactive oxygen species by polymorphonuclear leukocytes and mononuclear cells. Am J Clin Nutr. 2002;75:767–772.
36 Dandona P, Aljada A, Chaudhuri A, Mohanty P, Garg R. Metabolic syndrome: a comprehensive perspective based on interactions between obesity, diabetes, and inflammation. Circulation. 2005;111:1448–1454.
37 Rizvi AA. Inflammation markers as mediators of vasculo-endothelial dysfunction and atherosclerosis in the metabolic syndrome. Chin Med J (Engl). 2007;120:1918–1924.
38 Cai H, Harrison DG. Endothelial dysfunction in cardiovascular diseases: the role of oxidant stress. Circ Res. 2000;87:840–844.
39 Chalupsky K, Cai H. Endothelial dihydrofolate reductase: critical for nitric oxide bioavailability and role in angiotensin II uncoupling of endothelial nitric oxide synthase. Proc Natl Acad Sci U S A. 2005;102:9056–9061.
40 Evans JL, Maddux BA, Goldfine ID. The molecular basis for oxidative stress-induced insulin resistance. Antioxid Redox Signal. 2005;7:1040–1052.
41 Thiebaud D, Jacot E, DeFronzo RA, Maeder E, Jequier E, Felber JP. The effect of graded doses of insulin on total glucose uptake, glucose oxidation, and glucose storage in man. Diabetes. 1982;31:957–963.
42 DeFronzo RA, Jacot E, Jequier E, Maeder E, Wahren J, Felber JP. The effect of insulin on the disposal of intravenous glucose. Results from indirect calorimetry and hepatic and femoral venous catheterization. Diabetes. 1981;30:1000–1007.
43 Pendergrass M, Bertoldo A, Bonadonna R, Nucci G, Mandarino L, Cobelli C, et al. Muscle glucose transport and phosphorylation in type 2 diabetic, obese nondiabetic, and genetically predisposed individuals. Am J Physiol Endocrinol Metab. 2007;292:E92–E100.
44 Utriainen T, Takala T, Luotolahti M, Ronnemaa T, Laine H, Ruotsalainen U, et al. Insulin resistance characterizes glucose uptake in skeletal muscle but not in the heart in NIDDM. Diabetologia. 1998;41:555–559.
45 Guarino MP, Correia NC, Lautt WW, Macedo MP. Insulin sensitivity is mediated by the activation of the ACh/NO/cGMP pathway in rat liver. Am J Physiol Gastrointest Liver Physiol. 2004;287:G527–G532.
46 Guarino MP, Macedo MP. Co-administration of glutathione and nitric oxide enhances insulin sensitivity in Wistar rats. Br J Pharmacol. 2006;147:959–965.
47 Clark MG, Wallis MG, Barrett EJ, Vincent MA, Richards SM, Clerk LH, et al. Blood flow and muscle metabolism: a focus on

insulin action. Am J Physiol Endocrinol Metab. 2003;284:E241–E258.
48 Vincent MA, Clerk LH, Lindner JR, Klibanov AL, Clark MG, Rattigan S, et al. Microvascular recruitment is an early insulin effect that regulates skeletal muscle glucose uptake in vivo. Diabetes. 2004;53:1418–1423.
49 Russell-Jones D, Khan R. Insulin-associated weight gain in diabetes--causes, effects and coping strategies. Diabetes Obes Metab. 2007;9:799–812.
50 Scarpello JH. Improving survival with metformin: the evidence base today. Diabetes Metab. 2003;29:6S36–6S43.
51 Mamputu JC, Wiernsperger NF, Renier G. Antiatherogenic properties of metformin: the experimental evidence. Diabetes Metab. 2003;29:6S71–6S76.
52 Johnson M, Krosnick A, Carson P, McDade AM, Laraway K. A retrospective chart review of uncontrolled use of metformin as an add-on therapy in type 2 diabetes. Clin Ther. 1998;20:691–698.
53 Wu B, Fukuo K, Suzuki K, Yoshino G, Kazumi T. Relationships of systemic oxidative stress to body fat distribution, adipokines and inflammatory markers in healthy middle-aged women. Endocr J. 2009;56:773–782.
54 Pihl E, Zilmer K, Kullisaar T, Kairane C, Magi A, Zilmer M. Atherogenic inflammatory and oxidative stress markers in relation to overweight values in male former athletes. Int J Obes (Lond). 2006;30:141–146.
55 Piva SJ, Duarte MM, Da Cruz IB, Coelho AC, Moreira AP, Tonello R, et al. Ischemia-modified albumin as an oxidative stress biomarker in obesity. Clin Biochem. 2011;44:345–347.
56 Chrysohoou C, Panagiotakos DB, Pitsavos C, Skoumas I, Papademetriou L, Economou M, et al. The implication of obesity on total antioxidant capacity in apparently healthy men and women: the ATTICA study. Nutr Metab Cardiovasc Dis. 2007;17:590–597.
57 Hartwich J, Goralska J, Siedlecka D, Gruca A, Trzos M, Dembinska-Kiec A. Effect of supplementation with vitamin E and C on plasma hsCRP level and cobalt-albumin binding score as markers of plasma oxidative stress in obesity. Genes Nutr. 2007;2:151–154.
58 Milagro FI, Campion J, Martinez JA. Weight gain induced by high-fat feeding involves increased liver oxidative stress. Obesity (Silver Spring). 2006;14:1118–1123.
59 Tracy RP. Inflammation, the metabolic syndrome and cardiovascular risk. Int J Clin Pract Suppl. 2003:10–17.
60 Caballero AE. Metabolic and vascular abnormalities in subjects at risk for type 2 diabetes: the early start of a dangerous situation. Arch Med Res. 2005;36:241–249.
61 Galili O, Versari D, Sattler KJ, Olson ML, Mannheim D, McConnell JP, et al. Early experimental obesity is associated with coronary endothelial dysfunction and oxidative stress. Am J Physiol Heart Circ Physiol. 2007;292:H904–H911.